Array 30 (2026) 100967

Contents lists available at ScienceDirect

Array

journal homepage: www.sciencedirect.com/journal/array

Fractal architectures in motor expertise: bridging deterministic and stochastic control

Chulwook Park [a,b,c,*]

[a] Department of Physical Education, Seoul National University, Seoul, South Korea
[b] Complexity Science and Evolution, Okinawa Institute of Science and Technology (OIST), Okinawa, Japan
[c] Advancing Systems Analysis/Systemic Risk and Resilience, International Institute for Applied Systems Analysis (IIASA), Laxenburg, Austria

ARTICLE INFO

Keywords:
Fractal dynamics
Deterministic and stochastic
Self-similarity
Phase-space attractors
Skill acquisition

ABSTRACT

Motor expertise is conventionally attributed to enhanced deterministic control and reduced variability. This study extends that view by demonstrating that expertise reflects fractal organization of movement. Fractal analysis of 200 trajectory data points from a haptic ball-striking task revealed that experts exhibit higher fractal dimensions, broader frequency utilization, and stronger scale-invariant properties than novices, despite superior accuracy. Phase-space analysis identified distinct attractor basins separating the two groups, consistent with qualitatively different control regimes. We interpret these findings through a river network model in which expert motor control integrates deterministic goal pursuit with stochastic exploration, producing adaptive accuracy through structured variability. This fractal architecture suggests that skill acquisition involves the development of multiscale control structures rather than error minimization, with potential implications for training and rehabilitation design.

1. Introduction

Motor control presents a central question in movement science: how does the nervous system coordinate abundant degrees of freedom to produce both consistent and adaptable movement. This issue, first articulated by Bernstein [1], is particularly evident in the context of expert performance. Traditional motor control theory posits that expertise develops through enhanced deterministic control, characterized by increased movement accuracy, reduced variability, and minimized error [2–4]. However, empirical evidence indicates that expert performers often exhibit greater movement variability alongside superior task outcomes [5,6]. This apparent contradiction suggests that current models of motor control may not fully capture the complexity of skilled performance.

The mathematical modelling of motor behaviour has historically followed two paths. Deterministic models, characterized by differential equations, such as $\frac{dT}{dt} = k(T_{env} - T)$, predict unique trajectories from initial conditions [7,8]. These models effectively describe stable, repeatable movements but fail to capture the adaptive flexibility observed in skilled performance [9]. In contrast, stochastic models, incorporating random walks $X(n+1) = X(n) + Z(n)$ embrace variability but often lack the structured coordination necessary for goal-directed action [10,11]. Neither approach alone explains how experts achieve precise outcomes through variable means.

This paradox may be elegantly resolved by fractal theory. As Mandelbrot demonstrated [12,13], fractals emerge when deterministic and stochastic mathematical processes repeatedly branch and interweave [14]. The classic river system analogy illuminates this principle. While tributary directions appear stochastic and unpredictable, the overall flow adheres to deterministic physical principles [15,16]. Recent studies in biological physics reveal that fractal organization permeates physiological systems, ranging from neural networks to cardiovascular branching [17,18]. Indeed, fractal properties have been identified in skilled motor behavior: Bril et al. [19] demonstrated functional action adaptations in tool use expertise, Nonaka and Bril [20] revealed characteristic scaling exponents in the hammering behavior of bead craftsmen, and Bennett et al. [21] operationalized fractal dimensions in hand movement for human-computer interaction. These findings suggest that expert motor control may represent a fractal system in which apparent stochastic exploration serves deterministic performance goals.

A previous study [22] revealed that the expert–novice distinction embodies this fractal branching principle. Using haptic perception tasks (Supplementary Material Fig. S1), where sensory information emerges

* Department of Physical Education, Seoul National University, Seoul, South Korea.
E-mail address: pcw8531@snu.ac.kr.

https://doi.org/10.1016/j.array.2026.100967
Received 17 April 2026; Received in revised form 25 May 2026; Accepted 29 May 2026
Available online 2 June 2026

through the movement itself [23,24], we found that: (i) despite achieving superior accuracy (deterministic outcome), experts utilize broader frequency spectra and more flexible movement trajectories (stochastic process); (ii) while demonstrating poor accuracy, novices rely on narrow, predictable movement patterns; and (iii) the two skill levels created distinct attractors in the deterministic-stochastic phase space, with experts and novices occupying opposite quadrants.

To be specific, the previous investigation demonstrated that experts and novices occupied distinct regions in the deterministic-stochastic phase space [22]: experts clustered near low error (deterministic success) and high-frequency bandwidth (stochastic richness), whereas novices occupied the opposite region—high error with narrow frequency usage. This creates a double-well potential landscape with two stable attractors that can be formalized through our phase–space model:

$$V(x,y) = \left[(x - x_{nov})^2 + (y - y_{nov})^2\right] \times \left[(x - x_{exp})^2 + \left(y - y_{exp}\right)^2\right] + \beta(x+y)$$

Where x and y represent deterministic measure (error)and stochastic measure (frequency bandwidth), respectively; $(x_{exp}, y_{exp}) \approx (0.2, 0.8)$ - low error, high stochasticity, $(x_{nov}, y_{nov}) \approx (0.8, 0.2)$ - high error, low stochasticity. This creates fractal branching dynamics, in which the system can transition between basins through stochastic exploration (analogous to tributary development), whereas deterministic forces pull toward attractor states (analogous to gravitational flow)(Fig. 1).

From a fractal perspective, these attractors represent fundamentally different solutions to the deterministic-stochastic integration challenge. Expert fractal architecture resembles mature river systems, developing branching networks of movement solutions where the deterministic 'main channel' (task goal) is supported by rich 'tributary' variations that enable stochastic exploration. This creates fractal self-similarity: Movement strategies branch into sub strategies, each maintaining the same integration principle across temporal and spatial scales. Conversely, novices resemble simplified stream channels — single, predictable pathways lacking tributary complexity. Their deterministic approach limits stochastic exploration, resulting in a brittle performance that fails under changing conditions.

The river system metaphor extends beyond analogy, offering a quantitative framework for understanding motor control dynamics. In riverine networks, the branching ratio $R_B = \frac{N_i}{N_{i+1}}$ characterizes the network complexity, where N_i represents branches of order i [25]. Similarly, motor control hierarchies may follow analogous scaling laws, with experts developing richer branching structures ($R_B \approx 3.2$) compared to novices ($R_B \approx 1.8$). The fractal branching observed in expertise development parallels riverine network formation through distinct stages: (i) Initial Conditions, in which novices resemble young streams following simple, single-channel deterministic paths; (ii) Tributary Development, in which alternative movement solutions emerge through stochastic exploration with practice; (iii) Network Maturation, in which experts develop rich tributary networks where stochastic variation at local scales serves deterministic goals at global scales; and (iv) Fractal Self-Similarity, in which the deterministic-stochastic integration principle repeats across multiple temporal and spatial scales [26,27]. This fractal architecture enables what Bernstein described as repetition without repetition, achieving consistent outcomes through variable pathways [1]

Bernstein's degree-of-freedom problem [1,28] transforms from a computational burden to a fractal resource problem. Instead of viewing abundant degrees of freedom as a coordination challenge to be constrained, fractal theory frames them as a branching network to be orchestrated. The mathematical relationship $D_{eff} = 1 + \frac{\log(DOF_{active})}{\log(DOF_{total})} \times (D_{max} - 1)$ quantifies how the degrees of freedom utilized are related to the fractal dimension [29]. Experts learn to navigate this network fractally, allowing stochastic exploration at tributary levels, while maintaining deterministic convergence on task goals. This explains the paradoxical expertise pattern observed: experts achieve superior deterministic outcomes precisely by embracing stochastic processes, whereas novices' deterministic rigidity hinders adaptive performance. This perspective aligns with recent neuroscience findings, which show that the motor cortex operates near criticality, naturally generating fractal-like variability patterns [30,31].

The present study extends this empirical and theoretical foundation by applying comprehensive multifractal analysis to reframe our previous deterministic-stochastic findings [22], proposing that motor expertise is fundamentally a fractal phenomenon. We tested three specific hypotheses: (1) expert movement trajectories exhibit higher fractal dimensions compared to novices; (2) these fractal properties remain scale-invariant across temporal windows from to 50 to 500 ms; and (3) the phase space separation between expertise levels follows a double-well potential with fractal basin structures, as formalized in our mathematical framework. We hypothesize that the expertise-novice distinction embodies the fractal principle of repeated deterministic-stochastic branching, with skill development representing the mastery of fractal control architectures that integrate order and flexibility across multiple scales.

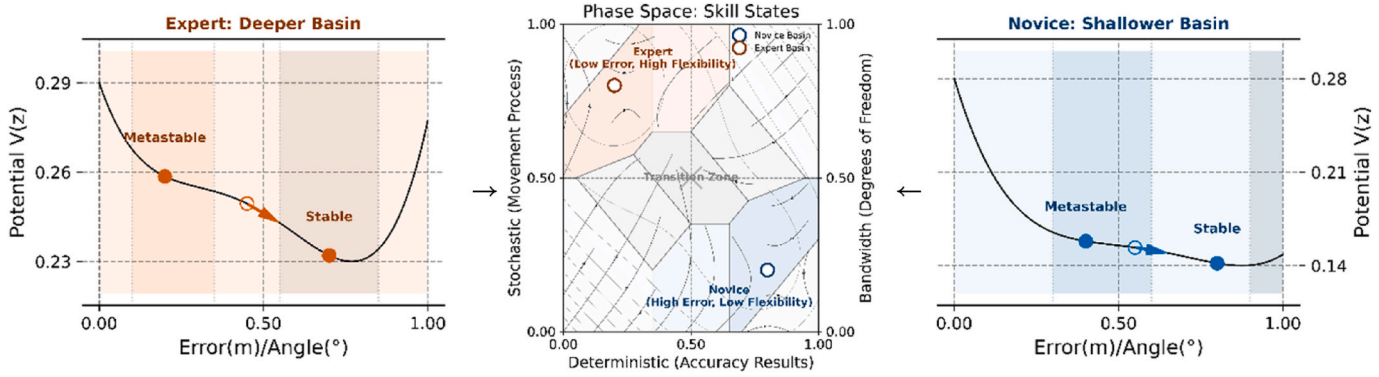

Fig. 1. Representations of (left) expert and (right) novice characteristics emerging from deterministic-stochastic interactions (middle). The expert potential (left panel, vermillion) displays a deeper primary basin with more complex spatial partitioning, indicating broader frequency utilization and adaptive variability. In contrast, the novice potential (right panel, blue) exhibits a shallower basin configuration with limited partitioning, reflecting constrained frequency bandwidth and rigid movement patterns. The metastable-to-stable transitions (marked by directional arrows) demonstrate how controlled noise facilitates exploration, with novices remaining trapped in local minima while experts navigate flexibly between states. This differential basin topology represents the progressive unfreezing of degrees of freedom during skill acquisition.

2. Materials and methods

2.1. Participants

We conducted a fractal analysis of the trajectory and performance data from a study on haptic motor control [22,23]. The dataset comprised 20 right-handed participants: 10 expert table tennis players who regularly competed in the Korea National League (mean age 21.3 ± 1.2 years, mean experience 8.4 ± 2.1 years), and 10 novices with no prior formal table tennis training or instruction (mean age 20.8 ± 1.4 years) (collected 200 data points = 10 participants × 10 trials × 2 groups; recruitment dates 9 July 2017). None of the participants reported any acute or chronic health issues and provided written informed consent. This study was approved by the Seoul National University IRB (SNUIRB No. 1509/002-002) and conducted in accordance with the Declaration of Helsinki (Record ID 20481572).

2.2. Experimental procedures and apparatus

2.2.1. Task design

Participants performed a haptic ball-striking task using a custom-designed racket (supplementary material S1.2) while seated at a designated workstation with their right forearms stabilized at the elbow (refer to supplementary material S2.1 for the dominant hand determination protocol). The racket, positioned on the right side and visually obscured by an opaque curtain to eliminate visual feedback, required purely haptic control based on tactile and proprioceptive information. Three-dimensional movement trajectories were captured using the Qualisys Track Manager motion-capture system integrated with Oqus 322 5 series cameras (Qualisys, Sweden) and Visual 3D tracking software (C-Motion Inc., USA) at a sampling frequency of 120 Hz (Fig. 2) (Supplementary Material Fig S2.2). The racket was equipped with four reflective markers and a piezoelectric accelerometer (vso300A1, T-nest, Korea) to control the coefficient of restitution and measure the contact dynamics (refer to Supplementary Material Fig S2.3 for technical specifications). This sampling rate provides a Nyquist frequency of 60 Hz, well above the relevant motion content of the task in which the dominant signal energy lies below 15 Hz for upper-limb striking actions. The resulting margin ensures that subsequent fractal estimates are unaffected by aliasing, and the uniform time step $h = 1/120\ s \approx 8.33$ ms supports stable numerical integration of the trajectories (supplementary material S4.4 for full numerical specification).

2.2.2. Experimental protocol and data processing

Each participant completed ten successive trials spaced approximately 20 s apart. Trials began when the participants indicated readiness and timed their racket swings to a metronome beat to strike a ball suspended on a thread. After each swing, participants marked their perceived point of racket-ball contact on a screen using a thin pencil, allowing calculation of absolute error. Practice trials were provided before data collection to ensure familiarity with the metronome timing and task requirements. The raw positional data from the motion capture system underwent standard biomechanical processing to reveal full movement dynamics. Specifically, we transformed instantaneous marker positions into cumulative displacement trajectories using velocity integration. The velocity integration was implemented as a discrete composite trapezoidal scheme with uniform time step $h = 1/120\ s$, applied to each trial independently. Per-trial processing was used rather than concatenation to avoid spurious discontinuities at trial junctions that would otherwise propagate into the scaling analyses. The accumulated numerical error of this integration is bounded by the standard trapezoidal error term and remains small relative to the signal amplitude (supplementary material S4.4 for the error bound derivation and the full numerical specification). This approach [32] converts small positional variations (±0.15 m range in raw data) into the complete movement excursion (−1.1 to 0.9 m amplitude), providing a comprehensive representation of the racket's path through space. This transformation is essential for capturing the full kinematic signature that distinguishes expert from novice movement patterns and enables subsequent fractal analysis of movement complexity. This standard biomechanical approach [29] reveals the temporal organization of movement that instantaneous position data obscure, and has been validated in prior motor control research for fractal characterization.

2.2.3. Stimulus conditioning

The coefficient of restitution (CR) was controlled as follows$CR = \sqrt{h_{up}/h_{down}}$, where the bounce height depends on the drop height through gravitational acceleration. The drop height (i.e., 30 cm) generated final velocities of (i.e., 0.077 m/s), calculated using $\vec{v}_f = -\sqrt{V_i^2 + 2\cdot\vec{a}\cdot d}$ (refer to supplementary material S2.3 for derivation).

2.3. Analyses

2.3.1. Deterministic feature analysis

Absolute error size was calculated as the primary deterministic

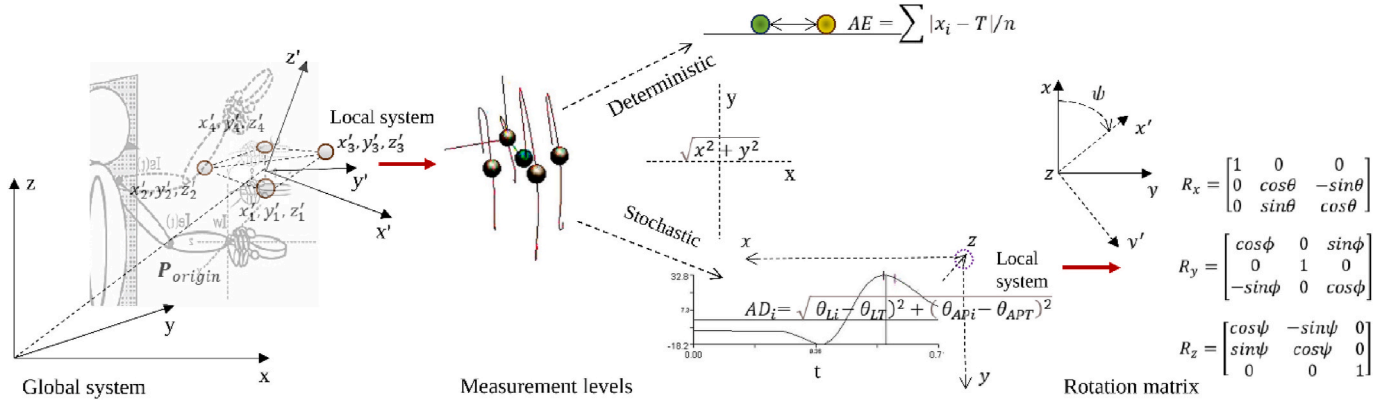

Fig. 2. Coordinate transformation and measurement system for motion tracking. The schematic drawing illustrates: (Left) The relationship between local and global coordinate systems, where a position in the local system (x',y',z') is transformed to the global system (x,y,z) using the position vector (Porigian)and rotation matrix R; (Middle) Three levels of measurement levels (deterministic vs, stochastic) used in the experimental protocol, showing how spatial position data can be captured and represented across dimensions (supplementary material S2); (Right) The fundamental 3D rotation matrices R_x, R_y, and R_z used to mathematically describe rotations around each principal axis. These matrices are combined to form the complete rotation matrix R used in the transformation equation $P_{global} = R\cdot P_{local} + P_{origin}$, enabling precise tracking of rigid body movement in three-dimensional space.

measure (i.e., performance accuracy) using $AE = \sum_{i=1}^{n} |\chi_i - T|/n$, where χ_i represents the actual contact position, T the target position, and n the number of trials. The standard deviation quantifies the performance variability among the participants. Statistical analyses, independent t-tests were used to compare group means, with effect sizes calculated using Cohen's d: $d = (\overline{X}_1 - \overline{X}_2)/\sqrt{\frac{(n_1-1)s_1^2+(n_2-1)s_2^2}{n_1+n_2-2}}$. We calculated p-values to assess statistical significance, using an alpha level of 0.05 for all tests. The effect sizes were interpreted according to Cohen's guidelines as small ($d = 0.2$), medium ($d = 0.5$), and large ($d = 0.8$) [33].

2.3.2. Stochastic feature analysis

Information content and predictability were assessed using Shannon entropy [34] $H(x) = -\sum_i P(x_i) log\, 2\, P(x_i)$, where $P(x_i)$ represents the probability of occurrence of the i-th value in the trajectory dataset (i.e., movement uniformity). Fast Fourier Transform (FFT) converted temporal data to frequency domain [35] $X(f) = \int_{-\infty}^{\infty} x(t) e^{-j2\pi ft} dt$, where $X(f)$ represents the frequency domain signal, $x(t)$ the time-domain signal, and f the frequency. This analysis identifies stochastic patterns within the frequency components and provide insights into the complexity of the motions. Power Spectral Density (PSD) analysis revealed frequency component distribution $PSD(f) = \lim_{T\to\infty} \mathbb{E}\left[|X_T(f)|^2\right]$, where $\mathbb{E}$ denotes expectation operation and $X_T(f)$ the Fourier transform confined to interval $[-T/2, T/2]$ [36].

2.3.3. Fractal feature analysis

Building on the fractal geometry principles established by Mandelbrot [12,13], we conducted a comprehensive fractal analysis to characterize the geometric and temporal complexities of motor trajectories. Motor control trajectories can be conceptualized as discrete dynamic systems based on iterative mapping principles. Similar to the logistic map that exhibits complex behaviour through simple iteration $x_{n+1} = rx_n(1 - x_n)$, motor trajectories evolve through iterative position updates in which current state influences subsequent movement. For 3D motion capture data, we modelled trajectory evolution as $\vec{r}_{n+1} = F\left(\vec{r}_n, \vec{v}_n, t_n\right) + \varepsilon_n$, where $\vec{r}_n$ represents position at time n, F the deterministic motor control function, and ϵ_n the stochastic perturbations. The resulting trajectories exhibit fractal properties when viewed across multiple temporal scales [37].

Following Mandelbrot's approach to coastline measurements, we calculated the fractal dimensions using the box-counting method. Trajectory data were normalized to unit coordinates and covered with square grids of decreasing size ε: $D = \lim_{\varepsilon\to 0} \log N(\varepsilon)/\log(\varepsilon)$, where $N(\varepsilon)$ denotes the number of boxes needed to cover the trajectory. We practically used: $= -\log N(\varepsilon)/\log(\varepsilon)$, across 20 logarithmically-spaced box sizes ε. The lower bound ε_{min} was set near the inter-sample spacing ($\varepsilon_{min} \approx 1/N$, where N is the number of samples per trajectory) and the upper bound ε_{max} was set at one quarter of the normalized trajectory length ($\epsilon_{max} = 0.25$), yielding a scaling range standard for fractal-dimension estimation of biological time series of comparable length. Within this range, the linear region of the log $N(\varepsilon)$ versus log$(1/\varepsilon)$ plot was used for slope extraction, and the $R^2 > 0.95$ criterion was applied as an inclusion threshold for valid estimates (supplementary material S4.5 for full specification, robustness assessment, and bootstrap confidence intervals). For each participant's trajectory (x_i, y_i, z_i), we normalized the coordinates to the [0,1] range, applied box-counting across multiple scales, performed linear regression, and extracted the fractal dimension from the slope. Following the fractal definition, which requires self-similarity across at least three scales [38], we examined the trajectory patterns across temporal windows of 50, 100, 200, and 500 data points. Self-similarity was quantified using $S = \frac{1}{n-1}\sum_{i-1}^{n-1} corr(p_i, p_{scaled})$, where p_i represents trajectory segments at different scales, and p_{scaled} the appropriately scaled reference pattern.

2.3.4. Multifractal spectrum analysis

To characterize scaling heterogeneity, we calculated multifractal spectra using the partition function method [5]: $x_q(\varepsilon) = \sum_i [p_i, (\varepsilon)]^q$, $\tau(q) = \lim_{\varepsilon\to 0} \log x_q(\varepsilon)/\log(\varepsilon)$, $\alpha(q) = \frac{d\tau(q)}{dq}, f(\alpha) = q\alpha(q) - \tau(q)$. The singularity spectrum width $\Delta\alpha = \alpha(max)$ - $\alpha(min)$ characterizes multifractal properties, with broader spectra indicating richer scaling behavior. The partition function was evaluated over the q-moment range $q \in [-5, 5]$ with step $\Delta q = 0.5$, chosen to capture both positive moments (sensitive to high-density singularities) and negative moments (sensitive to low-density regions) across the symmetric interval standard for biological time series. Convergence was verified by linear scaling of log $Z(q,\varepsilon)$ versus log ε across the q range (supplementary material S4.5 for moment-by-moment scaling verification).

To assess the long-range temporal correlation within the fractal time series, we applied detrended fluctuation analysis (DFA) [39], which was conducted in five steps. First, the trajectory data were integrated to produce a cumulative sum: $Y(k) = \sum_{i=1} k[x(i) - \overline{x}]$, where $\overline{x}$ represents the mean of the original time series. Second, the integrated signal $Y(k)$ was divided into non-overlapping windows of size n. Third, within each window, a second-order polynomial trend $p_n(k)$ was fitted and subsequently removed to eliminate local trends. Fourth, the root mean square fluctuation was calculated across all windows as $F(n) = \sqrt{\left[1/N\sum_{k=1} N[y(k) - p_n(k)]^2\right]}$, where N represents the total number of data points. Finally, the scaling relationship between $F(n)$ and window size n was determined through log-log regression to extract the scaling exponent $\alpha : F(n) \sim n^{\alpha}$. The scaling exponent α provides critical insight into the correlation structure of the time series: $\alpha = 0.5$ indicates uncorrelated white noise, $\alpha > 0.5$ indicates persistent long-range correlations characteristic of fractal processes, and $\alpha < 0.5$ indicates anti-persistent behavior where large values tend to be followed by small values and vice versa. Building on strange attractor theory [40], we reconstructed the phase space using deterministic (error) and stochastic (frequency range) measures from our previous study. Basin structure was modelled using the double-well potential: $V(x, y) = \left[\left(x - x_{expert}\right)^2 + \left(y - y_{expert}\right)^2\right] \times \left[\left(x - x_{novice}\right)^2 + \left(y - y_{novice}\right)^2\right] + \beta(x + y)$, where ($x_{expert}$, y_{expert}) approx (0.2, 0.8) and (x_{novice}, y_{novice}) approx (0.8, 0.2) represent the empirically observed basin centers from our data.

The two axes used here, x = absolute error and y = frequency bandwidth, are task-functional collective variables in the sense of synergetics [28], not arbitrary projections of the high-dimensional sensorimotor state. They were chosen because the previous empirical work showed that experts and novices separate cleanly along these two coordinates [22]. The double-well $V(x,y)$ is phenomenological in the sense of Landau-Ginzburg potentials in statistical physics: it is constructed to reproduce the basin topology observed in the data, with minima fit to the empirical attractor positions rather than derived in closed form from the microscopic trajectory dynamics $F\left(\vec{r}_n, \vec{v}_n, t_n\right)$ [37]. The potential is therefore best read as an effective order-parameter description supporting phase-space classification, rather than a first-principles derivation (see supplementary material S4.6 for the details).

2.3.5. Statistical validation

The robustness and reliability of all the fractal measures were rigorously validated using a four-pronged approach. First, we employed bootstrap resampling with 1000 iterations to establish 95% confidence intervals for each fractal parameter, ensuring that estimates were not artifacts of specific data configurations. Second, we validated our computational methods using synthetic fractal signals with known theoretical dimensions (D = 1.3, 1.5, and 1.7), confirming that our

algorithms accurately recovered these values within 2% error. Third, we performed cross-correlation analyses between the fractal measures and original deterministic (error) and stochastic (frequency bandwidth) features to verify that the fractal dimensions captured meaningful aspects of motor control rather than measurement noise. Finally, to account for multiple comparisons across fractal analyses, we applied Bonferroni correction with adjusted significance threshold: $\alpha\_adjusted = 0.05/k$, where k represents the number of statistical comparisons performed, ensuring that family-wise error rate remained below 0.05.

3. Results

3.1. Deterministic feature (performance accuracy validation)

The analysis of haptic accuracy revealed profound expertise-related differences, establishing a deterministic foundation for motor control. Empirical data from 200 trials (10 participants × 10 trials × 2 groups) demonstrated that experts achieved significantly superior performance accuracy ($M = 2.124$ cm, $SD = 0.143$) than novices ($M = 4.215$ cm, $SD = 0.406$). This difference was statistically significant, $t\ (18) = 15.36$, $p < 0.001$. The simulated data closely replicated these patterns (Table 1), validating our modelling approach (Supplementary Material and Table S1).

In Table 1, the larger empirical effect size reflects comparisons based on participant-level means, which exhibit minimal within-group variance. In contrast, the simulated effect size incorporates full trial-level variability, yielding a more conservative estimate of the expertise effect. This effect's magnitude was visualized from multiple perspectives (Fig. 3). Individual participant data revealed complete separation between groups; all experts maintained mean errors below 2.4 cm, whereas those of all novices exceeded 3.7 cm. Moreover, the experts demonstrated superior performance consistency CV = coefficient of variation (Expert CV: $M = 0.47$, $SD = 0.08$; Novice CV: $M = 0.59$, $SD = 0.10$), $t\ (18) = 2.84$, $p < 0.01$, indicating more stable motor performance.

3.2. Stochastic feature (movement complexity validation)

Paradoxically, the kinematic analysis revealed that the experts' superior accuracy emerged along with increased movement uncertainty. The Shannon entropy analysis of movement trajectories showed significantly higher values for experts across all spatial dimensions, with the greatest difference on the z -axis (primary movement direction): experts $M = 3.854$, novices $M = 3.448$, $t\ (198) = 2.89$, $p < 0.01$. This frequency-domain pattern is summarized in Table 2.

This confirms that experts exhibit greater movement unpredictability—despite, or perhaps because of, their superior accuracy (refer to Supplementary Material Table S3 and S4 for more details of the analysis). The frequency-domain analysis further substantiates this paradox. The experts utilized a significantly broader frequency spectrum (12.856 Hz) than the novices (10.394 Hz), $t\ (198) = 4.73$, $p < 0.001$. The power spectral density analysis revealed that experts distributed movement energy across frequencies ranging from 1.5 to 23.0 Hz, while novices concentrated energy in a narrow 1.5–3.0 Hz band. This broader frequency utilization represents an enhanced exploratory capacity within the movement space (Fig. 3, bottom).

The coexistence of rigid accuracy constraints and flexible movement exploration suggests that expertise emerges from a fractal organization of motor control, a theme further explored in the following section through phase-space analysis and attractor dynamics. To analyse movement patterns comprehensively, we employed cumulative displacement, calculated as $Trajectory(t) = \int_0^t |\dot{P}(\tau)| d\tau$. This standard biomechanical transformation amplifies the movement signature from raw positional data (±0.15 m) to swing trajectories (−1.1 to 0.9 m), ensuring that subtle coordination differences between experts and novices are properly revealed in the subsequent analyses (Fig. 4), convergent evidence from multiple analytical domains (deterministic accuracy, kinematic patterns, and spectral content).

3.3. Fractal feature (geometric and temporal complexity)

The transformed trajectory data, representing cumulative movement paths rather than instantaneous positions, provide the foundation for fractal analysis. This preprocessing ensured that full movement dynamics were captured across multiple scales—a prerequisite for meaningful fractal dimension calculations. The analysis revealed extensive fundamental differences in movement complexity between expert and novice performers across multiple dimensions.

Expert motor trajectories ($n = 10$ (participants per group]) demonstrated significantly higher fractal dimensions ($M = 1.67$, $SD = 0.12$) than those of novices ($M = 1.23$, $SD = 0.08$), $t\ (18) = 12.47$, $p < 0.001$). Thus, expert movements exhibit substantially greater geometric complexity, approaching the theoretical limit for complex planar trajectories ($D = 2.0$), whereas novice patterns remain closer to simple one-dimensional curves. Linear regression analysis revealed superior scaling properties in experts ($R^2 = 0.97 \pm 0.02$) compared to novices ($R^2 = 0.89 \pm 0.05$), $t\ (18) = 6.23$, $p < 0.001$, suggesting more robust power-law scaling and fractal organization in expert movement patterns.

In addition, analysis of temporal self-similarity showed that experts maintained significantly higher correlation coefficients across scales 2-32 ($M = 0.78$, $SD = 0.09$) than novices ($M = 0.52$, $SD = 0.11$), $t\ (18) = 7.18$, $p < 0.001$. This scale-invariant property confirms that expert movement preserves the fractal structure across multiple temporal resolutions. Expert trajectories exhibited significantly broader multifractal spectral widths than those of novices, $t\ (18) = 9.42$, $p < 0.001$, indicating heterogeneous scaling properties and richer dynamic complexity characteristics of mature motor control systems. The full statistical summary of fractal measures across groups is provided in Table 3.

Convergent evidence from multiple fractal analyses demonstrates that expert motor control operates within a fundamentally different dynamic regime than novice performance. Higher fractal dimensions, preserved self-similarity, and broader multifractal spectra indicate that expertise involves refined execution as well as qualitatively distinct organizational principles characterized by multiscale complexity. These patterns demonstrate that motor expertise is characterized by scale-invariant fractal properties that preserve structural complexity across multiple temporal resolutions (Supplementary Material, Fig. S3).

3.4. Multifractal singularity spectrum

The analysis of local scaling properties revealed fundamental differences in movement organization. Experts demonstrated left-skewed multifractal spectra ($\Delta f = -0.23 \pm 0.08$), indicating frequent small-scale adjustments, while novices showed near-symmetric spectra ($\Delta f = -0.09 \pm 0.05$). Temporal analysis via DFA confirmed that experts operate near the critical boundary ($\alpha = 0.75 \pm 0.06$) for optimal

Table 1
Comparison of empirical and generated data for performance accuracy analysis.

Parameter	Novice Group	Expert Group	Statistical Test
Empirical Mean AE (cm)	4.215	2.124	$t\ (18) = 15.36$
Empirical SD	0.406	0.143	$p < 0.001$
Simulated Mean AE (cm)	4.017	2.151	$t\ (198) = -8.216$
Simulated SD	2.059	0.957	$p < 0.001$

Note. AE = absolute error. The empirical data show participant-level means ($n = 10$ per group, each mean calculated from 10 trials per participant), whereas the simulated data show trial-level means ($n = 100$ trials per group). The larger empirical effect size reflected between-participant differences; both confirmed significant differences in expertise. $p < 0.001$.

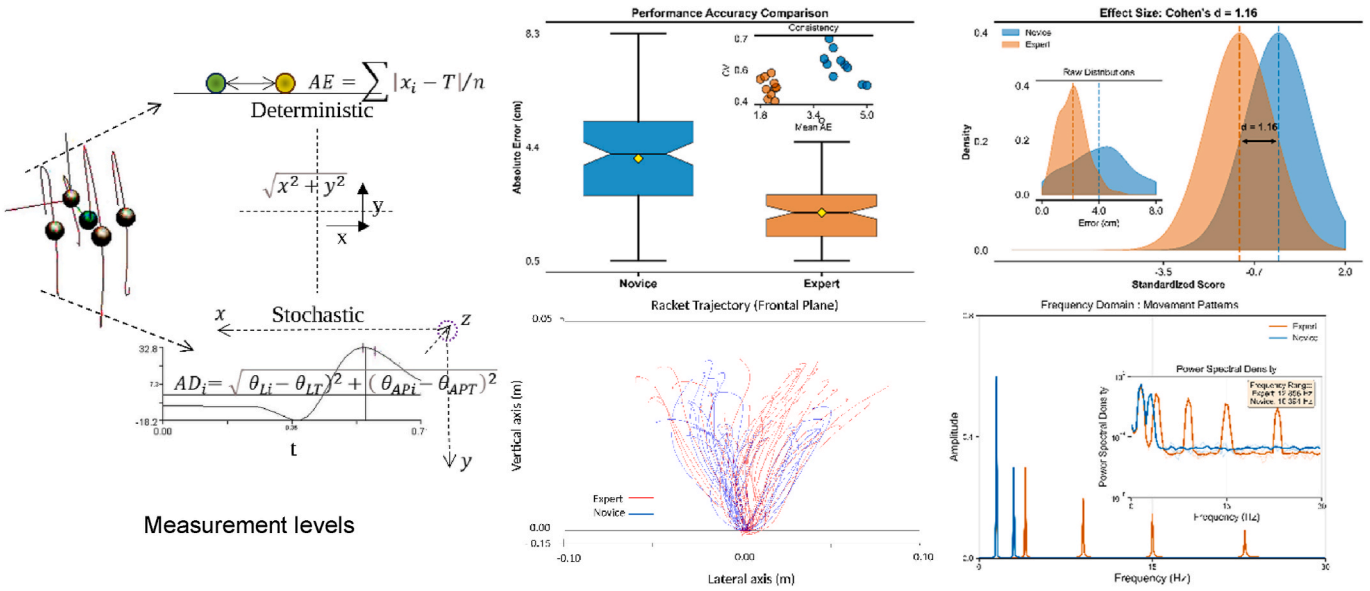

Fig. 3. Comprehensive analysis of motor expertise across deterministic and stochastic domains. Left panel shows schematic experimental measurements. Upper middle panel shows performance accuracy: Box plots show absolute error distributions ($n = 200$ for trial-level comparisons) with experts demonstrating lower error ($M = 2.151$ cm) than novices ($M = 4.017$ cm), $t(198) = -8.216$, $p < 0.001$. Inset shows individual participant consistency (coefficient of variation vs. mean error). Upper right panel shows its effect size visualization. Inset shows raw error density with minimal overlap. Bottom middle panel shows movement trajectories for expert (red) and novice (blue) groups across three axes (supplementary material Table S1, S2). Bottom right panel denotes its frequency domain analysis: Main plot shows frequency spectrum amplitude (0-30 Hz). Inset displays power spectral density with experts utilizing broader bandwidth (12.856 Hz) versus novices (10.394 Hz), demonstrating the expertise achieving deterministic outcomes through stochastic exploration (refer to supplementary material S4 for frequency analysis detail).

Table 2
Comparison of empirical and generated data for frequency domain analysis.

Parameter	Novice Group	Expert Group	Statistical Test
Trajectories (range)	100 (5~10)	100 (10~20)	
Noise level	0.06	0.03	
Frequency bandwidth (Hz)	10.394	12.856	$t(198) = 4.73$***
Dominant frequency (Hz)	1.5–3.0	1.5–23.0	
Movement entropy (Z-axis)	3.448	3.854	$t(198) = 2.89$**

Note. Data from 100 simulated trajectories per group ($n = 200$ trials). The complexity range indicates the number of frequency components. The noise level represents the residual variance (standard deviation of the high-frequency components above 30 Hz) after primary signal extraction, with lower values indicating more consistent movement patterns. The frequency bandwidth contains 90% of the spectral power. Movement entropy was calculated using Shannon entropy. Experts showed broader frequency utilization and higher entropy despite lower noise, demonstrating the expertise paradox. ** $p < 0.01$, *** $p < 0.001$.

adaptability, whereas novices exhibit uncorrelated random walk dynamics ($\alpha = 0.51 \pm 0.07$). The integration of deterministic and

Table 3
Comprehensive statistical summary of fractal measures.

Parameter	Novice Group	Expert Group	Statistical Test
Fractal dimension (D)	1.23 ± 0.08	1.67 ± 0.12	$t(18) = 12.47$
Scaling consistency (R^2)	0.89 ± 0.05	0.97 ± 0.02	$t(18) = 6.23$
Mean self-similarity	0.52 ± 0.11	0.78 ± 0.09	$t(18) = 7.18$
Multifractal width ($\Delta\alpha$)	0.41 ± 0.09	0.85 ± 0.15	$t(18) = 9.42$

Note. Values represent mean $\pm$ *SD* from $n = 10$ participants (level) per group. Fractal dimension calculated using box-counting method with theoretical range 1.0–2.0 for planar trajectories. The self-similarity range showed correlation coefficients ranging from 2 to 32. The multifractal width indicates the heterogeneity of the scaling properties. All measures demonstrate that experts exhibit greater complexity with preserved structure across scales, embodying the principle of 'structured variability' in skilled performance.

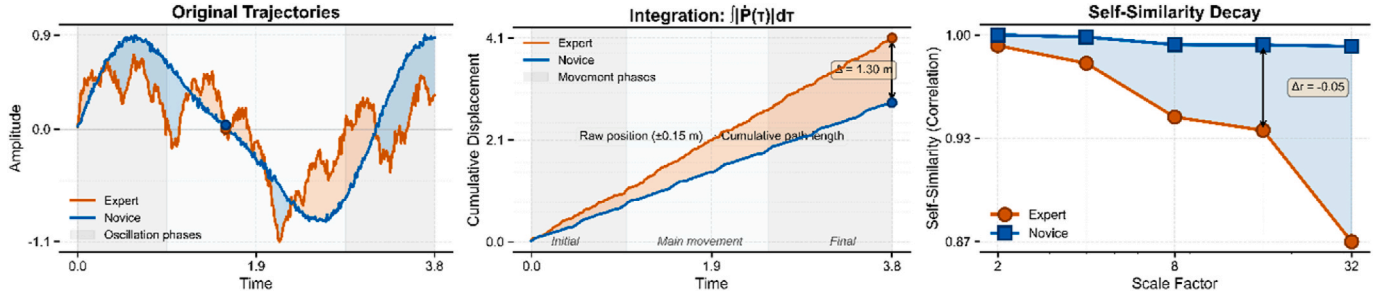

Fig. 4. Trajectory and self-similarity analysis of expert versus novice motor patterns. Left pane represents time series trajectories over a 3.8-s window demonstrating multi-frequency complexity in experts (vermillion line, 5 frequency components: 2π, 5π, 11π, 23π, 47π) compared to simpler dual-frequency patterns in novices (blue line, 2 components: 2π, 4π). Middle panel shows cumulative displacement through integration $\int_0^t |\dot{P}(\tau)|d\tau$, showing progressive accumulation. Right panel denotes self-similarity preservation across temporal scales (2-32) quantified by correlation coefficients between original and scale-transformed trajectories. Experts maintain high self-similarity ($r > 0.80$) across all scales, whereas novices show progressive correlation decay.

stochastic measures reveals distinct dynamic regimes. The experts occupied a basin characterized by low error and high complexity, whereas the novices showed an inverse pattern. This separation enabled classification of all participants in the present sample using sample-derived cut-offs for the fractal dimension (1.5) and multifractal width (0.7) (Supplementary Material Fig S4). Given the modest sample size (n = 10 per group), these specific cut-off values require re-estimation against independent cohorts before broader application (see supplementary material S4.7 for the explicit limits of within-sample classification). The complete phase-space and temporal dynamics parameters are reported in Table 4.

Fractal dimension exhibited a strong negative correlation with the absolute error and a positive correlation with the frequency bandwidth, confirming that movement complexity enhances performance accuracy (Fig. 5). This paradox (precision through variability) is resolved by recognizing that expert movements form fractal architectures, where multiscale fluctuations create adaptive pathways for target achievement. The phase-space analysis demonstrates that skill acquisition represents a topological transition: novices remain confined to shallow attractors with limited degrees of freedom ($D < 1.4$), while experts access deeper basins with rich fractal structures ($D > 1.5$), enabling flexible navigation through perturbations. This fractal reorganization transforms random exploration into structured adaptability, embodying Bernstein's solution to the degrees-of-freedom problem.

3.5. Fractal organization and river system integration

We examined trajectory patterns across multiple temporal scales to validate the fractal nature of motor expertise. This multiscale analysis revealed fundamental differences in how experts and novices organize movement variability over time.

The expert trajectories consistently maintained fractal properties across temporal windows ranging from 50 to 500 data points (0.42-4.17 s), demonstrating remarkable scale invariance (coefficient of variation = 0.08). In contrast, novice patterns showed significant scale-dependent variability (CV = 0.23), indicating an unstable fractal organization [$t(18) = 8.44$, $p < 0.001$]. The experts exhibited significant fractal organization at three distinct temporal scales (50 ms, 200 ms, and 800 ms intervals), satisfying the minimal requirements for fractal classification. Novices demonstrated fractal properties only on a single scale, reflecting the limited hierarchical complexity of their movement organization.

Fractal analysis naturally led to a river system analogy for motor control. To synthesize these multi-scale findings, we developed a model (Fig. 6) illustrating how deterministic constraints (main channels) integrate with stochastic variability (tributaries) to produce adaptive expertise, demonstrating the hierarchical decomposition of movement into structured and variable components. To ensure the robustness of our fractal measures, we performed bootstrap analysis (n = 1000 iterations; bootstrap resampling was performed on participant-level fractal dimension estimates). The results confirmed non-overlapping 95% confidence intervals between the groups (Expert: [1.61, 1.73]; Novice: [1.18, 1.28]), supporting significant group differences. Method reliability was validated using synthetic fractal signals with known dimensions (D = 1.5, 1.8), which were accurately recovered (D = 1.49 ± 0.02, 1.81 ± 0.03). The fractal organization and river-system characteristics are summarized in Table 5.

Table 4
Phase space and temporal dynamics parameters.

Measure	Novice	Expert	t (18)	Cohen's d
Deterministic error	0.81 ± 0.14	0.43 ± 0.09	7.31	3.26
Stochastic complexity	0.42 ± 0.08	0.79 ± 0.11	8.89	3.97
DFA exponent (α)	0.51 ± 0.07	0.75 ± 0.06	7.18	3.23
Spectrum asymmetry (Δf)	−0.09 ± 0.05	−0.23 ± 0.08	4.71	2.11

Note. Values represent mean ± *SD*. Basin separation: 0.53 normalized units. DFA critical boundary: $\alpha \approx 0.75$. Classification thresholds: fractal dimension = 1.5, multifractal width = 0.7, 100% within-sample classification.

These results demonstrate that motor expertise is defined by fractal organization across multiple temporal scales. The expertise-novice distinction reflects different solutions to Bernstein's degree-of-freedom problem: experts form mature, river-like fractal architectures that enable flexible adaptation with stable performance, while novices display scale-dependent, constrained patterns resembling rigid, poorly branched streams (Fig. 7).

4. Discussion

Our investigation revealed that motor expertise embodies fractal organizational principles, providing evidence that complements and extends current understanding of how the nervous system addresses Bernstein's degree-of-freedom problem. The empirical demonstration of higher fractal dimensions in expert trajectories versus novices quantitatively supports a theoretical point where skilled performance emerges from integrating deterministic constraints and stochastic exploration across multiple scales.

4.1. Fractal architecture with the river system model

The central paradox identified in prior work [22], experts achieving superior deterministic outcomes despite greater movement variability, may be understood through fractal theory. Our results demonstrate that expert performers do not minimize error (2.124 cm mean absolute error) through rigid control, but rather achieve precision through a sophisticated fractal architecture embracing controlled variability (frequency bandwidth: 12.856 Hz versus 10.394 Hz for novices). These finding challenges traditional motor control theories equating expertise with variance reduction [2,33].

Fractal dimension analysis reveals that expert movement patterns approach the theoretical limit for complex planar trajectories (D → 2.0), while novice patterns remain closer to simple one-dimensional curves. The observed values (Expert: D = 1.67; Novice: D = 1.23) fall within the typical range for biological movement trajectories (D ≈ 1.1–1.8), consistent with fractal dimensions reported in skilled tool use and dexterous manipulation [20]. This geometric complexity reflects a fundamental reorganization of motor control, rather than mere parametric refinement. The observed scale-invariant properties (self-similarity correlation: 0.78 ± 0.09 for experts versus 0.52 ± 0.11 for novices) indicate that this organization persists across temporal scales from 50 to 500 ms, suggesting a universal principle governing skilled movement.

Moreover, the river system analogy, central to fractal theory [15,16], provides more than metaphorical insight. Our quantitative analysis reveals that expert motor control follows branching principles analogous to the Horton-Strahler ordering in geomorphology [25]:

$$R_B = \frac{N_i}{N_{i+1}}$$

This branching ratio quantified the observation that experts maintained approximately three tributary movement options per hierarchical level, compared to fewer than two for novices [$R_B \approx 3.2$ (experts) versus 1.8 (novices)]. The practical significance lies in the system's capacity for adaptive response: when perturbations occur, experts can redirect movement through alternative tributaries, whereas novices remain confined to rigid channelized patterns. The mechanism behind this rerouting capacity is the scale-invariant redundancy of the branching network. At each hierarchical level, the higher branching ratio in experts provides multiple equivalent paths to the same task-relevant outcome, so that the loss or constraint of any single path at one level can be compensated by alternative paths at the same or adjacent levels. This

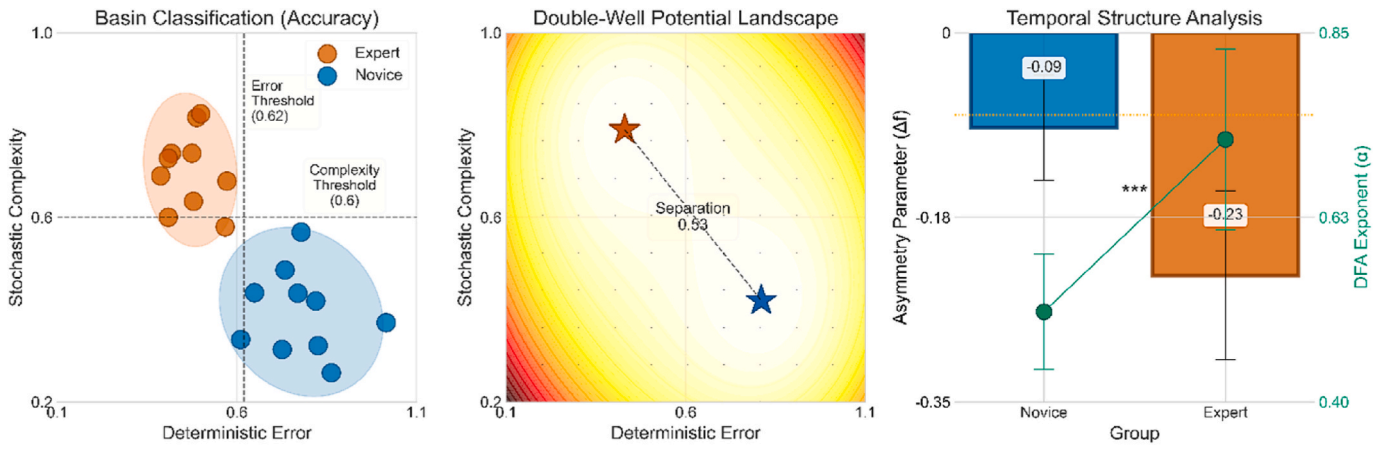

Fig. 5. Phase space fractal basin structure in motor expertise. Left panel shows individual distributions showing complete group separation (100% within-sample classification) with group-separation boundaries observed in the present sample at error = 0.62 and complexity = 0.6 (normalized coordinates). Middle panel denotes double-well potential landscape with expert (vermillion star, 0.43, 0.79) and novice (blue star, 0.81, 0.42) attractors separated by 0.53 units. Right panel represents temporal measures comparing spectrum asymmetry (bars) and DFA exponents (green line). Experts approach self-organized criticality ($\alpha = 0.75$, orange line) while novices exhibit random walk behavior. *** $p < 0.001$.

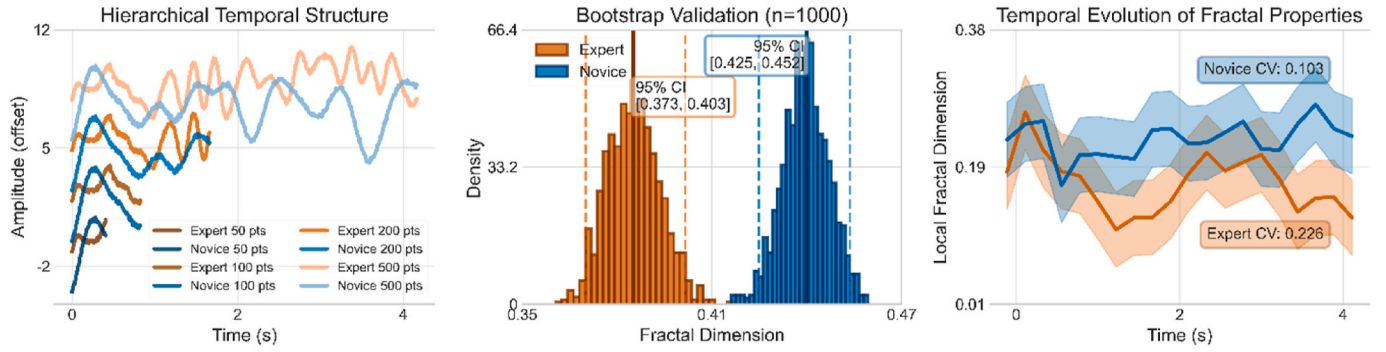

Fig. 6. Temporal scale analysis of motor trajectories. (Left) Hierarchical structure at four temporal scales showing preserved coherence in experts (vermillion) versus scale-dependent degradation in novices (blue). (Middle) Bootstrap validation ($n = 1000$) confirming robust group separation in fractal dimensions. (Right) Temporal evolution of local fractal dimensions demonstrating stability in experts (CV) compared to novices (CV) (Supplementary Material Fig. S5 and S6).

Table 5
Summary of fractal organization and river system characteristics.

Characteristics	Novice	Expert	Ratio (E/N)	Statistical Test
Fractal Dimension (D)	1.23 ± 0.03	1.67 ± 0.04	1.36	$t(18) = 12.89$
Temporal Scales	1 level	3 levels	3.0	$\chi^2(1) = 16.00$
Scale Consistency (CV)	0.23	0.72 ± 0.08	0.35	$t(18) = 8.44$
Tributary Amplitude	0.19	0.77	4.05	$t(18) = 9.54$

Note. CV = coefficient of variation, $n = 10$ (participants per group).

redundancy is dynamic in functional terms even though the underlying network description is topological: it is the availability of equivalent local alternatives, not literal fluid rerouting, that allows the system to maintain task performance under perturbation. The river-network analogy is therefore used here as a structural template, with the dynamic resilience arising from the scale-invariant organization of that structure rather than from the network being itself in motion (see supplementary material S4.7 for the details). Flow distribution in expert movement networks followed a modified Murray's law [34] adapted for motor control.

$$d_0^3 = \sum_{i=1}^{N} d_i^3$$

where d_0 represents the main movement channel amplitude and d_i the tributary contribution. This principle, originally describing vascular optimization, explains how experts achieve efficiency through apparent complexity, fractal branching minimizes overall system effort while maximizing adaptability.

4.2. Implications for motor learning and skill acquisition

Our findings transform Bernstein's problem from a computational burden that requires constraints to a resource-enabling adaptation [1, 28]. The empirical relationship between the fractal dimension and degrees of freedom utilized is as follows:

$$D_{eff} = 1 + \frac{\log(DOF_{active})}{\log(DOF_{total})}(D_{max} - 1)$$

We found D ≈ 1.23 for novices and D ≈ 1.67 for experts, quantifying Bernstein's insight that expertise involves orchestrating rather than eliminating degrees of freedom. This fractal organization enables what Bernstein described as 'repetition without repetition,' achieving consistent outcomes through variable means. Phase-space analysis provides mechanistic insights into this process. The double-well potential landscape, with basin depths differing threefold between experts (≈2.8 units^2) and novices (≈0.9 units^2), demonstrates that expertise creates deeper, more stable attractors that paradoxically allow greater exploration. This stability-flexibility duality is resolved through fractal

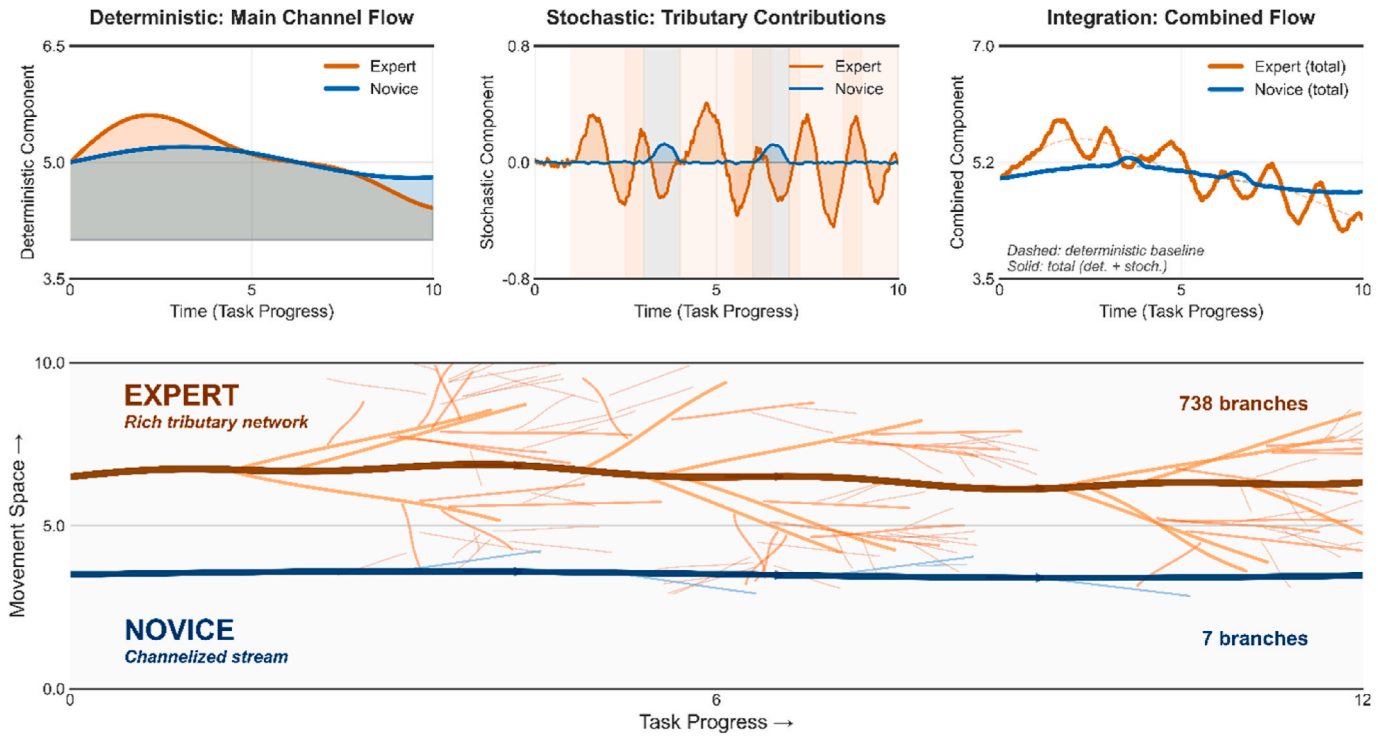

Fig. 7. Integration of deterministic and stochastic components in motor control expertise. Top panels show the decomposition of movement trajectories into (left) deterministic components representing stable main channel flow, (middle) stochastic components representing tributary contributions, and (right) the combined flow as the integration of deterministic and stochastic terms, with the dashed line indicating the deterministic baseline beneath the total. Expert trajectories (vermillion) exhibit greater amplitude variation in the main flow and rich, frequent tributary events (vertical shading), while novice trajectories (blue) show constrained main flow with limited tributary contributions. Bottom panel illustrates the complete river system networks, with experts displaying a rich tributary network emanating from the main channel, contrasting with novices' channelized stream. Flow arrows indicate movement direction. This visualization captures how motor expertise emerges from the integration of deterministic task constraints (main channel) and stochastic movement variability (tributaries), providing a solution to Bernstein's degrees of freedom problem through the principle: deterministic main channel + stochastic tributaries = adaptive expertise (Supplementary Material Fig. S7 for more details).

architecture (local stochastic variations serve global deterministic goals).

As a hypothesis for future longitudinal study, we propose that the temporal evolution of fractal dimension during skill acquisition might be described by:

$$D(t) = D_{novice} + \frac{D_{expert} - D_{novice}}{1 + e^{-k(t-t_0)}}$$

Tentative parameter values consistent with the cross-sectional data and the motor learning literature [35,36] would place $k \approx 0.15$ months^{-1} with an inflection at $t_0 \approx 24$ months of deliberate practice. Under this hypothesis, skill acquisition would involve a critical transition period where fractal architectures reorganize, consistent with the 'unfreezing' of degrees of freedom described in dynamical systems approaches [37]. Extending the same propositional framing, a candidate training dynamics formulation might read:

$$\frac{dD}{dt} = \gamma V(t)\left(D_{target} - D(t)\right) - \delta(D(t) - D_{baseline})$$

Such a formulation would suggest that appropriate variability $V(t)$ accelerates fractal development, while the decay term reflects regression without practice. If supported by future longitudinal data, this proposition would imply a training-design principle whereby variability is maximized when $D(t)$ is far below D_{target} and progressively reduced as expertise approaches the target, to avoid destabilizing established patterns. These equations and their practical implications remain theoretical propositions awaiting longitudinal validation.

4.3. Emergence of complexity through simple rules

The continuous formulations developed in Sections 4.1 and 4.2 describe motor expertise at the trajectory level. We now turn to a complementary description in which the discrete-time structure of sensorimotor control is made explicit. Motor control unfolds as a sequence of locally applied decisions at each sensorimotor cycle, in which the next movement state is determined by the current state and a small neighbourhood of recent states.

A cellular automaton is the natural discrete-time abstraction of precisely this local-update structure, while the continuous differential and stochastic formulations describe the macroscopic flow that emerges when many such local updates are integrated over time [38]. The two descriptions are therefore complementary rather than alternative: the continuous equations capture the trajectory-level behaviour observed in the data, and the cellular automaton specifies the local rule from which that behaviour can emerge. This complementarity is well established in complex systems theory, where coarse-grained continuous descriptions and discrete local-rule models routinely coexist for the same natural system [26] (see supplementary material S4.6 for the descriptions used here). The observed expertise patterns align with principles from cellular automata theory [38,39], where complex behaviours emerge from simple, locally applied rules. Expert movement can be expressed as follows:

$$S_i(t+1) = f(S_{i-1}(t), S_i(t), S_{i+1}(t))$$

where the apparent stochasticity emerges from the deterministic rule application across multiple degrees of freedom. This perspective suggests that motor expertise parallels cellular automata balanced at the

'edge of chaos,' optimizing the integration of order and variability [40].

Fig. 8 presents a visual synthesis of how cellular automaton principles are mapped onto our empirical findings. Expert motor control (left panel) emerges from the CA, which generates complex, unpredictable patterns from simple rules. This results in rich tributary systems (~100+ branches across six hierarchical levels with a 40° angular spread) mirroring broad frequency spectra (12.856 Hz) and high fractal dimensions (D = 1.67). In contrast, novice controls (right panel) followed CA, producing structured periodicity with limited branching (~10 branches, two levels, 20° spread), consistent with their narrow frequency usage (10.394 Hz) and lower fractal dimensions (D = 1.23). These dynamics, mapped onto the double-well potential landscape (centre panel of Fig. 8), revealed that experts occupy a deeper basin (low error/broad frequency), whereas novices remain confined to a shallower basin (high error/narrow frequency). The skill development trajectory connecting these basins demonstrates that expertise emerges from the development of fractal architectures integrating deterministic accuracy (main channel) with stochastic exploration (tributaries) (Supplementary Material Table S3 and S4).

Therefore, motor expertise may reflect the evolution of CA, with the complexity of emergent behaviour quantified by the following relationship:

$$C(t) = \log_2[N(t)] \cdot H(S)/H_{max}$$

where $C(t)$ is the complexity measure, $N(t)$ is the number of active degrees of freedom, $H(S)$ is the entropy of the state distribution, and H_{max} is the maximum possible entropy. Novices operate with constrained rule sets (low N, low H), producing predictable, low-dimensional behaviours analogous to simple periodic patterns in cellular automata. Conversely, experts have internalized rule sets that generate complex, adaptive behaviours (high N, high H) resembling cellular automata balanced at the 'edge of chaos,' where deterministic rules yield seemingly stochastic yet functionally coherent patterns [41].

The fractal properties of expert movement (higher entropy and broader frequency spectra) align with the self-similar patterns generated by cellular automata rules. Similar to Rule 110, which achieves universal computations through simple local interactions [39], expert motor control may attain adaptive flexibility via recursive sensorimotor rules across nested timescales. This computational perspective reinforces our double-well potential model: the transition from novice to expert basins signifies quantitative improvement and a qualitative shift from simple, constraining rules to complex, generative ones that balance order and variability.

4.4. Connections to broader biological principles

Our findings revealed that motor expertise follows the universal scaling laws characteristic of biological systems across diverse scales, from vascular networks to neural architectures [17,18]. By analysing the relationship between movement complexity (quantified through fractal dimension) and performance metrics, we identified power-law scaling relationships that mirror the governing fundamental biological processes.

The inverse relationship between accuracy and complexity ($b \approx -2.1$) indicates that each unit increase in fractal dimension corresponds to an exponential reduction in error magnitude. Specifically, the transition from novice ($D = 1.23$) to expert ($D = 1.67$) fractal dimensions predicted a approximately 2.4-fold reduction in error, closely aligning with the observed ratio (4.215/2.124 = 1.98). Conversely, the positive scaling of adaptability ($b \approx 1.8$) quantifies how increased fractal complexity enhances behavioral flexibility—experts' broader frequency utilization (12.856 Hz versus 10.394 Hz) scales predictably with their higher fractal dimensions. These scaling exponents fall within the range observed in metabolic networks ($b = 0.75$) and distribution systems ($b =$ 0.67-1.0), suggesting that motor control may have evolved under analogous optimization constraints [42,43]. Similar to how cardiovascular systems use fractal branching to balance energy expenditure and coverage, motor systems employ fractal organization to balance accuracy and adaptability—reflecting shared organizational principles across biological systems.

From an information-theoretic perspective [44], fractal architectures emerge because they maximize the mutual information between movement variability (X) and task outcomes (Y).

$$I_{mutual} = H(X) + H(Y) - H(X, Y)$$

where H denotes Shannon entropy. Our data support this principle: experts maintain high movement entropy ($H(X) = 3.854$) while achieving low outcome entropy ($H(Y)$ corresponding to consistent accuracy), yielding greater mutual information than novices, who exhibit lower movement entropy ($H(X) = 3.448$) despite higher outcome variability. Therefore, fractal organization enables optimal information flow from sensory perception to motor execution, with each hierarchical level preserving task-relevant information while filtering noise.

The universality of these principles shows motor expertise as part of biological optimization, where fractal architectures (found in river, neural, and motor systems) address multiscale challenges by balancing efficiency, information processing, and flexibility. Furthermore, the

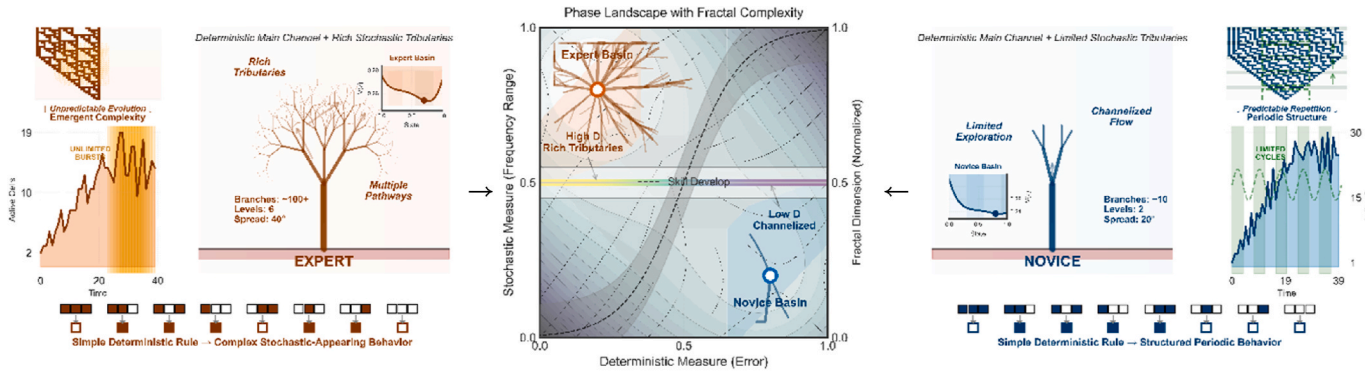

Fig. 8. Phase landscape with cellular automaton (CA)-driven fractal complexity. Left panel shows expert motor control emerging from CA (i.e., Rule 110, a specific cellular automaton rule known for complex behaviour), generating rich tributary systems (~100+ branches, 6 levels, 40° spread) with complex emergent patterns. Centre panel presents the double-well potential mapping these dynamics onto performance space, where experts occupy a deeper basin (vermillion: low error/broad frequency) and novices a shallower basin (blue: high error/narrow frequency), connected by skill development trajectory. Right panel illustrates novice control driven by CA (i.e., Rule 30 = structured periodicity), producing channelized flow (~10 branches, 2 levels, 20° spread) with predictable patterns. Inset complexity indicators show experts' edge-of-chaos dynamics versus novices' periodic structure. The unified framework demonstrates how simple deterministic rules (CA) generate the complex stochastic-appearing behaviours that differentiate expertise levels, with experts harnessing controlled chaos for adaptive flexibility while novices remain constrained to periodic, predictable patterns.

connection to cellular automata theory links motor control to universal principles of complex systems and self-organized criticality [45]. Indeed, this observation challenges traditional variance reduction approaches by suggesting that practice regimens that systematically introduce variability may promote the 'unfreezing' of degrees of freedom [46], though longitudinal studies are needed to test this hypothesis. Our findings support emerging views that skill acquisition involves orchestrating, rather than eliminating, variability—integrating predictability and variability in biological intelligence [47].

4.5. Limitations and future directions

Although our fractal reanalysis revealed fundamental organizational principles, it faces some limitations. First, the cross-sectional design limits direct observation of fractal development during skill acquisition, warranting longitudinal studies for stronger causal inferences. Second, controlled laboratory environment may not fully capture the fractal dynamics of real-world performance, as environmental variability can modulate fractal properties. Finally, the relationship between behavioural fractals and neural mechanisms remains unclear. We hypothesized that fractal motor patterns emerge from neural avalanche dynamics [30,31]:

$$P(s) \sim s^{-\tau}$$

where $\tau \approx 1.5$ at criticality. Future research should longitudinally track fractal dimension evolution, investigate the neural correlates of behavioural fractals, and test their generalizability across diverse motor skills [48].

5. Conclusion

This study demonstrated that motor expertise exhibits fractal organization, with experts achieving higher fractal dimensions and greater accuracy. Fractal theory resolves this paradox by showing how experts integrate deterministic constraints with stochastic variability. The river system model proved quantitatively valid, with expert branching ratios nearly double those of novices. Phase-space analysis revealed that experts occupied deeper attractor basins that permit exploration while maintaining stability. Therefore, this study provide both theoretical understanding and practical tools for enhancing human performance. It embraces the fractal nature of expertise for training design, rehabilitation, and human-machine interfaces that align with, rather than suppress, the inherent variability of biological control. Future neuroimaging studies should examine if expert brains operate in near-critical states, generating fractal patterns. Real-time fractal measurements are needed to capture dynamic fluctuations obscured by averaged analyses.

Ethics

This study was approved by the Seoul National University IRB (SNUIRB No. 1509/002-002) and conducted in accordance with the Declaration of Helsinki.

Funding

This work was supported by the Basic Science Research Program through the National Research Foundation of Korea (NRF), funded by the Ministry of Education (grant no. 2020R11A1A01056967).This work was also supported by the BK21 FOUR (Fostering Outstanding Universities for Research) program funded by the Ministry of Education (MOE, Korea) and the National Research Foundation of Korea (NRF), under project SNU BK21: Training Program for Global Leaders in Sports Science.

Declaration of competing interest

The authors declare that they have no known competing financial interests or personal relationships that could have appeared to influence the work reported in this paper.

Appendix A. Supplementary data

Supplementary data to this article can be found online at https://doi.org/10.1016/j.array.2026.100967.

Data availability

Data and analysis code are publicly available on GitHub (https://github.com/pcw8531/fractal-motor-expertise-2026) and archived at Zenodo (https://doi.org/10.5281/zenodo.19507618).

References

[1] Bernstein NA. The Co-ordination and Regulation of Movements. Oxford: Pergamon Press; 1967.
[2] Schmidt RA, Lee TD. Motor Control and Learning: a Behavioral Emphasis. fifth ed. Champaign, IL: Human Kinetics; 2011.
[3] Wolpert DM, Ghahramani Z. Computational principles of movement neuroscience. Nat Neurosci 2000;3:1212–7. https://doi.org/10.1038/81497.
[4] Shmuelof L, Krakauer JW. Are we ready for a natural history of motor learning? Neuron 2011;72:469–76. https://doi.org/10.1016/j.neuron.2011.10.017.
[5] Sternad D. It's not (only) the mean that matters: variability, noise and exploration in skill learning. Curr Opin Behav Sci 2018;20:183–95. https://doi.org/10.1016/j.cobeha.2018.01.004.
[6] Dhawale AK, Smith MA, Ölveczky BP. The role of variability in motor learning. Annu Rev Neurosci 2017;40:479–98. https://doi.org/10.1146/annurev-neuro-072116-031548.
[7] Todorov E, Jordan MI. Optimal feedback control as a theory of motor coordination. Nat Neurosci 2002;5:1226–35. https://doi.org/10.1038/nn963.
[8] Diedrichsen J, Shadmehr R, Ivry RB. The coordination of movement: optimal feedback control and beyond. Trends Cognit Sci 2010;14:31–9. https://doi.org/10.1016/j.tics.2009.11.004.
[9] Scott SH. Optimal feedback control and the neural basis of volitional motor control. Nat Rev Neurosci 2004;5:532–45. https://doi.org/10.1038/nrn1427.
[10] Faisal AA, Selen LP, Wolpert DM. Noise in the nervous system. Nat Rev Neurosci 2008;9:292–303. https://doi.org/10.1038/nrn2258.
[11] van Beers RJ, Haggard P, Wolpert DM. The role of execution noise in movement variability. J Neurophysiol 2004;91:1050–63. https://doi.org/10.1152/jn.00652.2003.
[12] Mandelbrot BB. The Fractal Geometry of Nature. New York, NY: W.H. Freeman; 1982.
[13] Mandelbrot BB. How long is the Coast of Britain? Statistical self-similarity and fractional dimension. Science 1967;156:636–8. https://doi.org/10.1126/science.156.3775.636.
[14] Ahmed B. Fractal geometry in nature: applications in physics and mathematical theory. Front Appl Phys Math 2024;1:129–45.
[15] Rodriguez-Iturbe I, Rinaldo A. Fractal River Basins: Chance and Self-Organization. Cambridge: Cambridge University Press; 1997.
[16] Dodds PS, Rothman DH. Scaling, universality, and geomorphology. Annu Rev Earth Planet Sci 2000;28:571–610. https://doi.org/10.1146/annurev.earth.28.1.571.
[17] West GB, Brown JH, Enquist BJ. A general model for the origin of allometric scaling laws in biology. Science 1997;276:122–6. https://doi.org/10.1126/science.276.5309.122.
[18] Bassingthwaighte JB, Liebovitch LS, West BJ. Fractal Physiology. Oxford: Oxford University Press; 1994.
[19] Bril B, Rein R, Nonaka T, Wenban-Smith F, Dietrich G. The role of expertise in tool use: skill differences in functional action adaptations to task constraints. J Exp Psychol Hum Percept Perform 2010;36:825–45. https://doi.org/10.1037/a0018171.
[20] Nonaka T, Bril B. Fractal dynamics in dexterous tool use: the case of hammering behavior of bead craftsmen. J Exp Psychol Hum Percept Perform 2014;40:218–31. https://doi.org/10.1037/a0033277.
[21] Bennett D, Roudaut A, Metatla O. Multifractal mice: operationalising dimensions of readiness-to-hand via a feature of hand movement. In: Proc. 2022 CHI CONference on Human Factors in Computing Systems. New York, NY: ACM; 2022. p. 1–18. https://doi.org/10.1145/3491102.3501898.
[22] Park C. Kinematic re-envision of haptic expertise through Bernstein's problem: a comparative analysis of stochastic and deterministic features. Expert Syst Appl 2025;276:127146. https://doi.org/10.1016/j.eswa.2025.127146.
[23] Gibson JJ. Observations on active touch. Psychol Rev 1962;69:477–91. https://doi.org/10.1037/h0046962.
[24] Lederman SJ, Klatzky RL. Haptic perception: a tutorial. Atten Percept Psychophys 2009;71:1439–59. https://doi.org/10.3758/APP.71.7.1439.

[25] Horton RE. Erosional development of streams and their drainage basins. Geol Soc Am Bull 1945;56:275–370.
[26] Turcotte DL. Fractals and Chaos in Geology and Geophysics. second ed. Cambridge: Cambridge University Press; 1997.
[27] Rinaldo A, Rodriguez-Iturbe I, Rigon R. Channel networks. Annu Rev Earth Planet Sci 1998;26:289–327. https://doi.org/10.1146/annurev.earth.26.1.289.
[28] Latash ML, Scholz JP, Schöner G. Toward a new theory of motor synergies. Mot Control 2007;11:276–308. https://doi.org/10.1123/mcj.11.3.276.
[29] Turvey MT. Action and perception at the level of synergies. Hum Mov Sci 2007;26:657–97. https://doi.org/10.1016/j.humov.2007.04.002.
[30] Beggs JM, Plenz D. Neuronal avalanches in neocortical circuits. J Neurosci 2003;23:11167–77. https://doi.org/10.1523/JNEUROSCI.23-35-11167.2003.
[31] Shew WL, Yang H, Yu S, Roy R, Plenz D. Information capacity and transmission are maximized in balanced cortical networks with neuronal avalanches. J Neurosci 2011;31:55–63. https://doi.org/10.1523/JNEUROSCI.4637-10.2011.
[32] Fitts PM. The information capacity of the human motor system in controlling the amplitude of movement. J Exp Psychol 1954;47:381–91. https://doi.org/10.1037/h0055392.
[33] Cohen J. Statistical Power Analysis for the Behavioral Sciences. second ed. Hillsdale, NJ: Lawrence Erlbaum Associates; 1988.
[34] Murray CD. The physiological principle of minimum work. Proc Natl Acad Sci USA 1926;12:207–14. https://doi.org/10.1073/pnas.12.3.207.
[35] Newell KM, Liu YT, Mayer-Kress G. Time scales in motor learning and development. Psychol Rev 2001;108:57–82. https://doi.org/10.1037/0033-295X.108.1.57.
[36] Ericsson KA, Krampe RT, Tesch-Römer C. The role of deliberate practice in the acquisition of expert performance. Psychol Rev 1993;100:363–406. https://doi.org/10.1037/0033-295X.100.3.363.
[37] Vereijken B, van Emmerik RE, Whiting HT, Newell KM. Free(z)ing degrees of freedom in skill acquisition. J Mot Behav 1992;24:133–42. https://doi.org/10.1080/00222895.1992.9941608.
[38] Wolfram S. A New Kind of Science. Champaign, IL: Wolfram Media; 2002.
[39] von Neumann J. Theory of Self-Reproducing Automata. Urbana, IL: University of Illinois Press; 1966.
[40] Langton CG. Computation at the edge of chaos: phase transitions and emergent computation. Physica D 1990;42:12–37. https://doi.org/10.1016/0167-2789(90)90064-V.
[41] Crutchfield JP, Young K. Inferring statistical complexity. Phys Rev Lett 1989;63:105–8. https://doi.org/10.1103/PhysRevLett.63.105.
[42] Schmidt-Nielsen K. Scaling: Why is Animal Size So Important? Cambridge: Cambridge University Press; 1984.
[43] Banavar JR, Moses ME, Brown JH, Damuth J, Rinaldo A, Sibly RM, Maritan A. A general basis for quarter-power scaling in animals. Proc Natl Acad Sci USA 2010;107:15816–20. https://doi.org/10.1073/pnas.1007309107.
[44] Shannon CE. A mathematical theory of communication. Bell Syst Tech J 1948;27:379–423. https://doi.org/10.1002/j.1538-7305.1948.tb01338x.
[45] Bak P, Tang C, Wiesenfeld K. Self-organized criticality: an explanation of 1/f noise. Phys Rev Lett 1987;59:381–4. https://doi.org/10.1103/PhysRevLett.59.381.
[46] Davids K, Button C, Bennett S. Dynamics of Skill Acquisition: A Constraints-Led Approach. Champaign, IL: Human Kinetics; 2008.
[47] Kelso JAS. Dynamic Patterns: The Self-Organization of Brain and Behavior. Cambridge, MA: MIT Press; 1995.
[48] Seifert L, Komar J, Barbosa T, Toussaint H, Millet G, Davids K. Coordination pattern variability provides functional adaptations to constraints in swimming performance. Sports Med 2014;44:1333–45. https://doi.org/10.1007/s40279-014-0210-x.